Introduction of wall effects into explicit algebraic stress models through elliptic blending

Abdou Gafari Oceni, Remi Manceau, Thomas B. Gatski

Introduction of wall effects into explicit algebraic stress models through elliptic blending

Abdou G. Oceni, Rémi Manceau, Thomas B. Gatski

1 Introduction

Explicit Algebraic Stress Models (EASMs) are a compromise between representation of the physics and numerical robustness. They inherit most of the capacities of the Reynolds stress model (RSM) from which they are derived to account for complex physical mechanisms. A corollary of the previous remark is that the EASMs also inherit some of the shortcomings of their underlying RSM; particularly, the influence of the blocking effect of the wall, which is not taken into account within the usual context of EASMs. The present work aims at incorporating in EASMs the elliptic blending method proposed by Manceau and Hanjalić [4, 2].

The Elliptic-Blending Reynolds-Stress Model (EB-RSM) aims at reproducing the blocking effect of the wall by enforcing the correct limiting behavior of the difference between the velocity–pressure-gradient and dissipation terms of the Reynolds stress (τ_{ij}) transport equation. The EB-RSM model is characterized by a simple blending between two asymptotically-correct forms of the model for $\phi^*_{ij} - \varepsilon_{ij}$

$$\phi^*_{ij} - \varepsilon_{ij} = (1-\alpha^2)\left[\phi^w_{ij} - \frac{\tau_{ij}}{k}\varepsilon\right] + \alpha^2\left[\phi^h_{ij} - \frac{2}{3}\varepsilon\delta_{ij}\right] \tag{1}$$

In order to reproduce the nonlocal character of the blocking effect, the blending function α is obtained from the elliptic relaxation equation

$$\alpha - L^2\nabla^2\alpha = 1, \tag{2}$$

with the boundary condition $\alpha = 0$, such that α goes from 0 at the wall to 1 far from the wall. ϕ^h_{ij} denotes hereafter the SSG [10] model, valid far from the wall. The analysis of the near-wall asymptotic behavior [4] shows that ϕ^w_{ij} must be of the

Abdou G. Oceni · Rémi Manceau · Thomas B. Gatski
Laboratoire d'études aérodynamiques (LEA), université de Poitiers, ENSMA, CNRS, Bd Marie et Pierre Curie, BP 30179, 86962 Futuroscope Chasseneuil Cedex, France, e-mail: remi.manceau@lea.univ-poitiers.fr

form

$$\phi_{ij}^{w} = -5\frac{\varepsilon}{k}\left[\tau_{ik}n_j n_k + \tau_{jk}n_i n_k - \frac{1}{2}\tau_{kl}n_k n_l\left(n_i n_j + \delta_{ij}\right)\right], \tag{3}$$

where $\boldsymbol{n}$ is a pseudo-wall-normal vector defined by $\boldsymbol{n} = \nabla\alpha/\|\nabla\alpha\|$. The present article describes the derivation and validation of explicit algebraic representations based on this Reynolds-stress model.

2 Explicit Algebraic Methodology

Using the weak equilibrium assumptions $\mathrm{d}b_{ij}/\mathrm{d}t = 0$ and $D_{ij}/D_{kk} = \tau_{ij}/\tau_{kk}$, where $b_{ij} = \tau_{ij}/(2k) - \delta_{ij}/3$ and D_{ij} are the anisotropy and the total diffusion of τ_{ij}, respectively, the following algebraic equation for the Reynolds stress is obtained

$$(P_{ij} - \frac{\tau_{ij}}{k}P) + \phi_{ij}^{*} - (\varepsilon_{ij} - \frac{\tau_{ij}}{k}\varepsilon) = 0. \tag{4}$$

Introducing the EB-RSM model into Eq. (4) yields, under tensorial form

$$\begin{gathered} -\frac{1}{a_4}\boldsymbol{b} - a_3\left(\boldsymbol{bS} + \boldsymbol{Sb} - \frac{2}{3}\{\boldsymbol{bS}\}\boldsymbol{I}\right) + a_2\left(\boldsymbol{bW} - \boldsymbol{Wb}\right) \\ \boxed{-a_5\left(\boldsymbol{bM} + \boldsymbol{Mb} - \frac{2}{3}\{\boldsymbol{bM}\}\boldsymbol{I} - \frac{1}{2}\{\boldsymbol{bM}\}\boldsymbol{M}\right)} = a_1\boldsymbol{S} + \boxed{\frac{a_5}{2}\boldsymbol{M}}, \end{gathered} \tag{5}$$

where $\{.\}$ denotes the trace, and $\boldsymbol{S}$ and $\boldsymbol{W}$ are the mean strain and mean rotation tensors, respectively. In Eq. (5) and henceforth, the enclosed terms are the terms due to the introduction of the elliptic blending procedure. These terms vanish far from the wall, where the parameter α goes to one. The a_i's are given by

$$\begin{gathered} a_1 = \frac{2}{3} - \frac{1}{2}(g_3 - \boxed{g_3^{*}\sqrt{1-\alpha^2}})\alpha^2, \quad a_2 = 1 - \frac{g_5}{2}\boxed{\alpha^2}, \quad a_3 = 1 - \frac{g_4}{2}\boxed{\alpha^2}, \\ a_4 = \frac{k}{\varepsilon}\left[(1 + \frac{g_1^{*}}{2}\boxed{\alpha^2})\frac{P}{\varepsilon} - (\boxed{\frac{13}{3}} - \frac{g_1}{2})\boxed{\alpha^2} + \boxed{\frac{13}{3}} - 1\right]^{-1}, \quad \boxed{a_5 = 5\frac{\varepsilon}{k}(1-\alpha^2)}, \end{gathered} \tag{6}$$

where the g_i's are the coefficients of the SSG model. Since the implicit algebraic system (5) is numerically intractable, an explicit solution must be sought. The theory of invariants [9] indicates that the solution of such a relation between tensors is a polynomial function of the tensors involved in the equation, of the form

$$\boldsymbol{b} = \sum_{i=1}^{N}\beta_i\boldsymbol{T}_i. \tag{7}$$

where $\boldsymbol{T}_i$ are the tensors of the so-called functional integrity basis, and the β_i's are polynomial invariant functions.

3 Invariant and functional integrity bases

The specificity of the present model lies in the presence of the tensor $\boldsymbol{M}$ in Eq. (5). Indeed, in the standard explicit algebraic methodology [7], the relation only involves $\boldsymbol{b}$, $\boldsymbol{S}$ and $\boldsymbol{W}$, such that the solution is of the form (7), in which the functional integrity basis consists of the $N = 10$ terms [7]

$$\begin{array}{c} \boldsymbol{T}_1 = \boldsymbol{S} \quad ; \quad \boldsymbol{T}_2 = \boldsymbol{SW} - \boldsymbol{WS} \quad ; \quad \boldsymbol{T}_3 = \boldsymbol{S}^2 - \frac{1}{3}\{\boldsymbol{S}^2\}\boldsymbol{I} \quad ; \quad \boldsymbol{T}_4 = \boldsymbol{W}^2 - \frac{1}{3}\{\boldsymbol{W}^2\}\boldsymbol{I} \quad ; \\ \boldsymbol{T}_5 = \boldsymbol{WS}^2 - \boldsymbol{S}^2\boldsymbol{W} \quad ; \quad \boldsymbol{T}_6 = \boldsymbol{SW}^2 + \boldsymbol{W}^2\boldsymbol{S} - \frac{2}{3}\{\boldsymbol{SW}^2\}\boldsymbol{I} \quad ; \quad \boldsymbol{T}_7 = \boldsymbol{WSW}^2 - \boldsymbol{W}^2\boldsymbol{SW} \quad ; \\ \boldsymbol{T}_8 = \boldsymbol{SWS}^2 - \boldsymbol{S}^2\boldsymbol{WS} \quad ; \quad \boldsymbol{T}_9 = \boldsymbol{W}^2\boldsymbol{S}^2 + \boldsymbol{S}^2\boldsymbol{W}^2 - \frac{2}{3}\{\boldsymbol{S}^2\boldsymbol{W}^2\}\boldsymbol{I} \quad ; \quad \boldsymbol{T}_{10} = \boldsymbol{WS}^2\boldsymbol{W}^2 - \boldsymbol{W}^2\boldsymbol{S}^2\boldsymbol{W}. \end{array} \tag{8}$$

The β_i's are polynomial functions of the terms of the invariant integrity basis

$$\eta_1 = \{\boldsymbol{S}^2\} \; ; \; \eta_2 = \{\boldsymbol{W}^2\} \; ; \; \eta_3 = \{\boldsymbol{S}^3\} \; ; \; \eta_4 = \{\boldsymbol{SW}^2\} \; ; \; \eta_5 = \{\boldsymbol{S}^2\boldsymbol{W}^2\} \; ; \; \eta_6 = \{\boldsymbol{SWS}^2\boldsymbol{W}^2\}. \tag{9}$$

In the present case, the relation (5) involves $\boldsymbol{b}$, $\boldsymbol{S}$, $\boldsymbol{W}$ *and* $\boldsymbol{M}$, such that the functional integrity basis now contains $N = 41$ terms and the invariant integrity basis 29 terms [9]. However, using the fact that $\boldsymbol{M}^2 = \frac{1}{3}\boldsymbol{M} + \frac{2}{9}\boldsymbol{I}$, the functional integrity basis reduces to $N = 27$ terms, i.e., Eq. (8) and the 17 additional terms

$$\begin{array}{c} \boldsymbol{T}_{11} = \boldsymbol{M} \quad ; \quad \boldsymbol{T}_{12} = \boldsymbol{SM} + \boldsymbol{MS} - \frac{2}{3}\{\boldsymbol{SM}\}\boldsymbol{I} \quad ; \quad \boldsymbol{T}_{13} = \boldsymbol{WM} - \boldsymbol{MW} \quad ; \\ \boldsymbol{T}_{14} = \boldsymbol{MWS} - \boldsymbol{SWM} - \frac{2}{3}\{\boldsymbol{MWS}\}\boldsymbol{I} \quad ; \quad \boldsymbol{T}_{15} = \boldsymbol{S}^2\boldsymbol{M} + \boldsymbol{MS}^2 - \frac{2}{3}\{\boldsymbol{S}^2\boldsymbol{M}\}\boldsymbol{I} \quad ; \\ \boldsymbol{T}_{16} = \boldsymbol{MW}^2 + \boldsymbol{W}^2\boldsymbol{M} - \frac{2}{3}\{\boldsymbol{MW}^2\}\boldsymbol{I} \quad ; \quad \boldsymbol{T}_{17} = \boldsymbol{W}^2\boldsymbol{MW} - \boldsymbol{WMW}^2 \quad ; \\ \boldsymbol{T}_{18} = \boldsymbol{WMS} - \boldsymbol{SMW} - \frac{2}{3}\{\boldsymbol{WMS}\}\boldsymbol{I} \quad ; \quad \boldsymbol{T}_{19} = \boldsymbol{WSM} - \boldsymbol{MSW} - \frac{2}{3}\{\boldsymbol{WSM}\}\boldsymbol{I} \quad ; \\ \boldsymbol{T}_{20} = \boldsymbol{WS}^2\boldsymbol{M} - \boldsymbol{MS}^2\boldsymbol{W} - \frac{2}{3}\{\boldsymbol{WS}^2\boldsymbol{M}\}\boldsymbol{I} \quad ; \quad \boldsymbol{T}_{21} = \boldsymbol{MWS}^2 - \boldsymbol{S}^2\boldsymbol{WM} - \frac{2}{3}\{\boldsymbol{MWS}^2\}\boldsymbol{I} \quad ; \\ \boldsymbol{T}_{22} = \boldsymbol{WMS}^2 - \boldsymbol{S}^2\boldsymbol{MW} - \frac{2}{3}\{\boldsymbol{WMS}^2\}\boldsymbol{I} \quad ; \quad \boldsymbol{T}_{23} = \boldsymbol{SWS}^2\boldsymbol{M} - \boldsymbol{MS}^2\boldsymbol{WS} - \frac{2}{3}\{\boldsymbol{SWS}^2\boldsymbol{M}\}\boldsymbol{I} \quad ; \\ \boldsymbol{T}_{24} = \boldsymbol{SW}^2\boldsymbol{M} + \boldsymbol{MW}^2\boldsymbol{S} - \frac{2}{3}\{\boldsymbol{SW}^2\boldsymbol{M}\}\boldsymbol{I} \quad ; \quad \boldsymbol{T}_{25} = \boldsymbol{W}^2\boldsymbol{SM} + \boldsymbol{MSW}^2 - \frac{2}{3}\{\boldsymbol{W}^2\boldsymbol{SM}\}\boldsymbol{I} \quad ; \\ \boldsymbol{T}_{26} = \boldsymbol{W}^2\boldsymbol{S}^2\boldsymbol{M} + \boldsymbol{MS}^2\boldsymbol{W}^2 - \frac{2}{3}\{\boldsymbol{W}^2\boldsymbol{S}^2\boldsymbol{M}\}\boldsymbol{I} \quad ; \quad \boldsymbol{T}_{27} = \boldsymbol{W}^2\boldsymbol{SWM} - \boldsymbol{MWSW}^2 - \frac{2}{3}\{\boldsymbol{W}^2\boldsymbol{SWM}\}\boldsymbol{I}, \end{array} \tag{10}$$

and the invariant integrity basis to 16 terms, i.e., Eq. (9) and the 10 additional terms

$$\begin{array}{c} \eta_7 = \{\boldsymbol{SM}\} \; ; \; \eta_8 = \{\boldsymbol{S}^2\boldsymbol{M}\} \; ; \; \eta_9 = \{\boldsymbol{W}^2\boldsymbol{M}\} \; ; \; \eta_{10} = \{\boldsymbol{WSM}\} \; ; \; \eta_{11} = \{\boldsymbol{WS}^2\boldsymbol{M}\} \; ; \; \eta_{12} = \{\boldsymbol{WS}^2\boldsymbol{MS}\} \; ; \\ \eta_{13} = \{\boldsymbol{W}^2\boldsymbol{SM}\} \; ; \; \eta_{14} = \{\boldsymbol{W}^2\boldsymbol{S}^2\boldsymbol{M}\} \; ; \; \eta_{15} = \{\boldsymbol{W}^2\boldsymbol{SWM}\} \; ; \; \eta_{16} = \{\boldsymbol{W}^2\boldsymbol{MWS}^2\}. \end{array} \tag{11}$$

The solution (7) of Eq. (5) can be obtained by performing a Galerkin projection, which leads to a 27×27 invertible linear system for the β_i functions.

4 Truncated bases

In order to reduce the complexity of the model, the usual approach, for instance followed by [8] for the SSG model, is to consider a 2D plane flow. In this case, it can be shown [7] that the functional integrity basis is reduced to the 3 terms $\boldsymbol{T}_1$–$\boldsymbol{T}_2$–$\boldsymbol{T}_3$, and the invariant integrity basis to η_1–η_2. The expression (7) with $N = 3$ is the solution of Eq. (5) in 2D plane cases only, and can be used as an approximation in 3D.

However, in our case, the integrity basis in 2D plane flows contains the 6 terms $\boldsymbol{T}_1$–$\boldsymbol{T}_2$–$\boldsymbol{T}_3$–$\boldsymbol{T}_{11}$–$\boldsymbol{T}_{12}$–$\boldsymbol{T}_{13}$, which leads to an overly complex model. Therefore, in the present paper, only bases consisting of at most 3 terms are used.

This restriction is not too severe, considering that in a 2D plane flow case, the anisotropy tensor is determined by only 3 independent parameters, b_{11}, b_{22} and b_{12}. However, since such a basis is not an integrity basis, the function (7) obtained by Galerkin projection can be singular at particular locations in the flow domain.

The standard choice for the 3-term basis is the 2D plane flow integrity basis $\boldsymbol{T}_1$–$\boldsymbol{T}_2$–$\boldsymbol{T}_3$. The use of this basis leads to a model denoted by EB-EASM #1 (First Elliptic Blending Explicit Algebraic Stress Model).

However, basis tensors involving the tensor $\boldsymbol{M}$ are attractive. Indeed, this tensor is independent of the mean field, and tensors such as $\boldsymbol{T}_{11}$, $\boldsymbol{T}_{12}$ and $\boldsymbol{T}_{13}$ are at most linear in the mean velocity gradient. This is a very desirable property for improving numerical robustness. Moreover, $\boldsymbol{M}$ carries the information about the orientation of the wall, which is crucial in its vicinity to ensure a correct representation of the anisotropy in 3D flows (where a 3-term basis representation of $\boldsymbol{b}$ is incomplete). Another interesting characteristic of $\boldsymbol{M}$ is that it does not vanish where $\boldsymbol{S}$ and $\boldsymbol{W}$ vanish.

Several combinations of models based on 2-, 3- and 5-term bases have been analytically investigated. The complexity of the formulation is only dependent on the number of tensors retained in the basis, not on the particular choice of the basis tensors. Using a 5-term basis may be valuable in 3D, complex flows, but at the price of a considerable increase of the complexity of the formulation. 4 different attractive choices for the basis have been identified, and the resulting models are

- EB-EASM #1: $\boldsymbol{b} = \beta_1 \boldsymbol{S} + \beta_2(\boldsymbol{SW} - \boldsymbol{WS}) + \beta_3(\boldsymbol{S}^2 - \frac{1}{3}\{\boldsymbol{S}^2\}\boldsymbol{I})$
- EB-EASM #2: $\boldsymbol{b} = \beta_1 \boldsymbol{S} + \beta_2 \boldsymbol{M}$
- EB-EASM #3: $\boldsymbol{b} = \beta_1 \boldsymbol{S} + \beta_2 \boldsymbol{M} + \beta_3(\boldsymbol{SM} + \boldsymbol{MS} - \frac{2}{3}\{\boldsymbol{SM}\}\boldsymbol{I})$
- EB-EASM #4: $\boldsymbol{b} = \beta_1 \boldsymbol{S} + \beta_2(\boldsymbol{SW} - \boldsymbol{WS}) + \beta_3 \boldsymbol{M}$

The reasons for selecting these particular models can be summarized as follows: EB-EASM #1 is the standard choice and can thus be easily compared with standard models, but it is nonlinear in the mean velocity gradient ; EB-EASM #2 is the simplest formulation (only 2 basis tensors) that preserves the two-component limit of turbulence at the wall ($b_{22} = -1/3$) ; EB-EASM #3 is linear in the mean velocity gradient, which is desirable for numerical robustness, but degenerates to EB-EASM #2 in 1D flows, since the last two tensors of the basis are linearly dependent in this situation ; EB-EASM #4 is not susceptible to this degeneracy, and incorporates the tensor $\boldsymbol{M}$, such that it does not degenerate where $\boldsymbol{S}$ and $\boldsymbol{W}$ vanish. In the following sections, the focus will be on 1D flows, where EB-EASM #3 and #4 are identical to EB-EASM #2 and #1, respectively. Thus, it will only be necessary to present results given by the models #1 and #2.

For a 2D plane flow, the Galerkin projection of Eq. (5) onto either one of the 4 bases selected in the previous section provides β_i's of the form

$$\beta_i \left(\eta, \mathscr{R}, \boxed{\mathscr{P}}, \boxed{\mathscr{Q}}, \frac{k}{\varepsilon}, \frac{P}{\varepsilon}, \boxed{\alpha} \right). \tag{12}$$

where $\eta = \sqrt{\eta_1} = \sqrt{\{\boldsymbol{S}^2\}}$ and $\mathscr{R} = \sqrt{-\eta_2/\eta_1} = \sqrt{-\boldsymbol{W}^2/\boldsymbol{S}^2}$ are the mean strain parameter and the mean kinematic vorticity number, respectively. The introduction of elliptic blending results in the appearance of two additional invariants in the models, $\mathscr{P} = \eta_7 = \{\boldsymbol{SM}\}$ and $\mathscr{Q} = 2\eta_{10} = 2\{\boldsymbol{WSM}\}$, that both characterize the orientation of the velocity gradient in the coordinate system linked to the wall. $\mathscr{P}$ is zero in a flow parallel to the wall and maximum at an axisymmetric impingement point, and $\mathscr{Q}$ is zero at an impingement point and maximum in a flow parallel to the wall. Therefore, $\mathscr{P}$ and $\mathscr{Q}$ are called the *Impingement invariant* and the *Boundary layer invariant*, respectively.

The dependence on k/ε, P/ε and α originates from the variable a_i coefficients of Eq. (6). k, ε and α are provided by their own differential equations, such that the original second-moment closure is reduced to a 3-equation model. The ratio of production to dissipation, P/ε, appears in Eq. (5) via a_4, and is a function of β_1, since $P/\varepsilon = -2\beta_1\eta^2 k/\varepsilon$. Consequently, β_1 is the solution of a nonlinear algebraic equation, that is cubic for the model EB-EASM #2, but *quartic* for the others. It is worth pointing out that this equation is only cubic in standard models using 3-term bases: the increase of the degree of the equation is due to the introduction of the elliptic blending method. This peculiarity does not make the selection of the proper root more problematic in the 1D cases under consideration in the present article, since there is a single physically admissible root (real and negative).

5 Validation of the models

The first validation test is the investigation of the analytical form of the models in a channel flow, in order to check that the models inherit from the EB-RSM the reproduction of the two-component limit of turbulence at the wall. In such a 1D flow, the invariants reduce to $\eta = \partial U/\partial y/\sqrt{2}$, $\mathscr{R} = 1$, $\mathscr{P} = 0$ and $\mathscr{Q} = \eta^2$, and it can be shown that the models EASM #1 and #2 yield

$$\boldsymbol{b} = \begin{bmatrix} -\beta_2\eta^2 + \frac{1}{6}\beta_3\eta^2 & \frac{\sqrt{2}}{2}\beta_1\eta & 0 \\ \frac{\sqrt{2}}{2}\beta_1\eta & \beta_2\eta^2 + \frac{1}{6}\beta_3\eta^2 & 0 \\ 0 & 0 & -\frac{1}{3}\beta_3\eta^2 \end{bmatrix} \text{ and } \boldsymbol{b} = \begin{bmatrix} -\frac{1}{3}\beta_2 & \frac{\sqrt{2}}{2}\beta_1\eta & 0 \\ \frac{\sqrt{2}}{2}\beta_1\eta & \frac{2}{3}\beta_2 & 0 \\ 0 & 0 & -\frac{1}{3}\beta_2 \end{bmatrix}, \quad (13)$$

respectively. In both models, $-k\beta_1$ plays the role of an eddy-viscosity. In model #1, β_2 and β_3 drive the anisotropy of the normal stresses, while in model #2, the use of a 2-term basis does not enable the reproduction of the full anisotropy of the normal stresses, leading to $b_{11} = b_{33}$ throughout the channel.

As the wall is approached ($y \to 0$), it can be shown that $\beta_1 \to 0$. For model #1, $\beta_2 \to -1/(4\eta^2)$ and $\beta_3 \to -1/(2\eta^2)$, while for model #2, $\beta_2 \to -1/2$. Therefore, for both models, the original limiting behavior of the EB-RSM ($b_{12} = 0$, $b_{22} = -1/3$, $b_{11} = b_{33} = 1/6$, $b_{12} = 0$) is preserved, and the two-component limit of turbulence is correctly enforced ($b_{22} = -1/3$). Such a favorable behavior with the linear, 2-term model #2 is noteworthy.

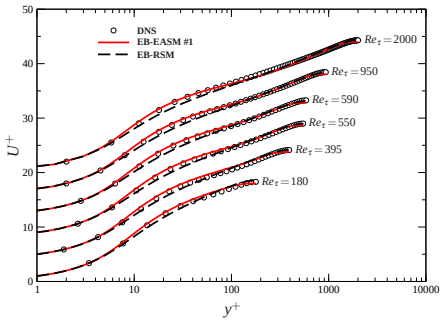

Fig. 1 EB-EASM #1: Mean velocity profiles in plane Poiseuille flows.

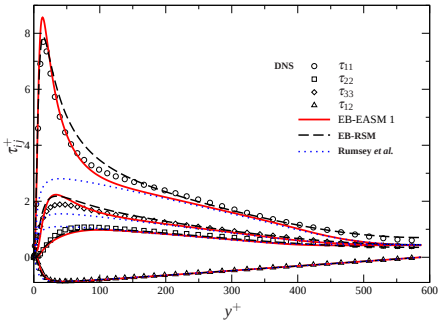

Fig. 2 EB-EASM #1: Reynolds-stress profiles in the plane Poiseuille flow at $Re_\tau = 590$.

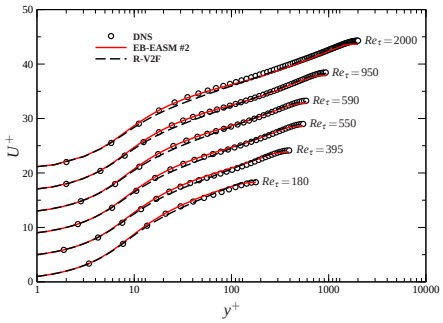

Fig. 3 EB-EASM #2: Mean velocity profiles in plane Poiseuille flows.

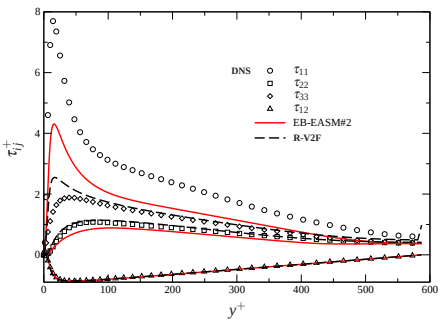

Fig. 4 EB-EASM #2: Reynolds-stress profiles in the plane Poiseuille flow at $Re_\tau = 590$.

Fig. 1 shows the mean velocity profiles given by EB-EASM #1 and its underlying RSM, the EB-RSM, in the case of Poiseuille flows at Reynolds numbers ranging from $Re_\tau = 180$ to 2000 [5, 1]. In Fig. 2, the corresponding Reynolds stresses at $Re_\tau = 590$ are shown. It is seen that the algebraic model gives profiles almost identical to the EB-RSM, except for the anisotropy at the channel center, due to the weak equilibrium hypothesis on the diffusion term. The Reynolds stresses given by the explicit algebraic model of [8] are also shown in Fig. 2. This model is identical to EB-EASM #1 far from the wall ($\alpha \to 1$), as highlighted in Eqs. (5)–(12). This comparison emphasizes the effect of the introduction of the elliptic blending method in the explicit algebraic formulation.

Figs. 3 and 4 show the same results for EB-EASM #2, compared to the rescaled-$\overline{v^2}$–f model [3]. As pointed out previously, the reproduction of the anisotropy is not complete since the wall-normal component $\overline{v^2}$ and the shear-stress $\overline{uv}$ are closely approximated, but the model yields exactly $\overline{u^2} = \overline{w^2}$ throughout the channel. This behavior is similar to that of the $\overline{v^2}$–f model, provided that the $\overline{v^2}$ component used for comparison is the one given by the additional "$\overline{v^2}$" equation, not by the Boussinesq relation.

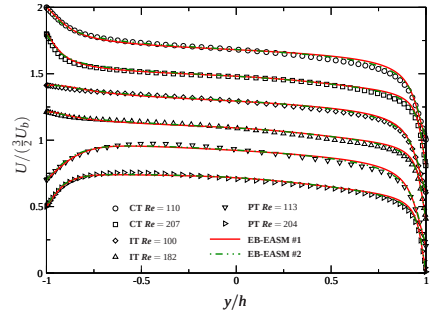

Fig. 5 Couette-Poiseuille flows: mean velocity profiles. PT, CT, IT denote Poiseuille-, Couette- and Intermediate-Type, respectively.

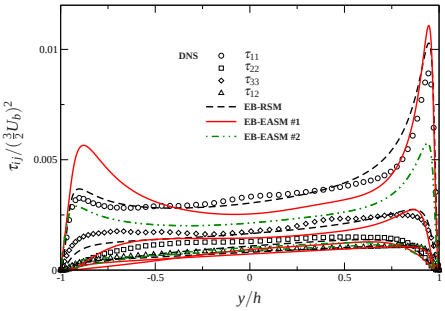

Fig. 6 Couette-type flow: Reynolds-stress profiles for $Re_\tau = 207$.

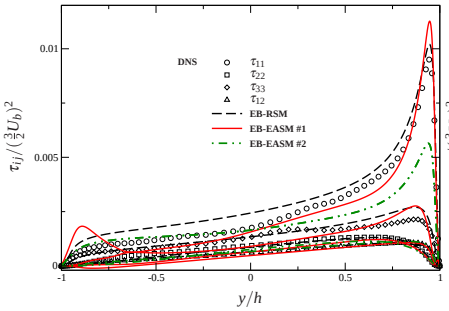

Fig. 7 Intermediate-type flow: Reynolds-stress profiles for $Re_\tau = 182$.

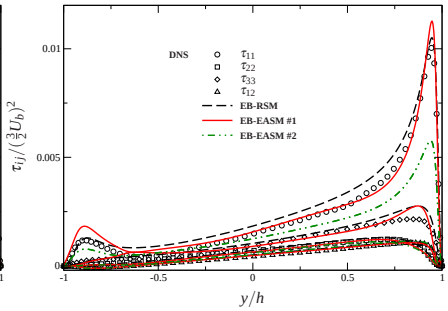

Fig. 8 Poiseuille-type flow: Reynolds-stress profiles for $Re_\tau = 204$.

Figs. 5–8 show the results obtained using EB-EASM #1, EB-EASM #2 and the EB-RSM, in Couette-Poiseuille flows, compared with the DNS data of Orlandi [6]. These 1D flows are generated by imposing a pressure gradient and a moving wall. Three different configurations are studied, distinguished by the velocity gradient at the moving wall: positive for the "Poiseuille-type" flow; negative for the "Couette-type" flow; and nearly zero for the "intermediate-type" flow. Two Reynolds numbers are studied for each configuration.

Fig. 5 shows the satisfactory reproduction of the mean velocity profiles by all the models, and in Figs. 6–8 it is shown that the EB-RSM reproduces the Reynolds stress very well for the 3 types of flows. The nonlinear model EB-EASM #1 gives satisfactory results overall, but overestimates the anisotropy in the vicinity of the moving wall, in particular for the Couette-type flow. In such a 1D flow, this discrepancy necessarily comes from the use of the weak equilibrium hypothesis for the diffusion terms: in the region close to the moving wall, the relative weight of these terms is increased due to the reduction of the turbulent level.

The results given by EB-EASM #2 are comparable to those shown previously for Poiseuille flows. The crucial components $\overline{uv}$ and $\overline{v^2}$ are correctly reproduced; although, $\overline{u^2} = \overline{w^2}$ is obtained. It is worth pointing out that EB-EASM #2 actually

better approximates $\overline{uv}$ and $\overline{v^2}$ than EB-EASM #1 in the intermediate-type flow. This can be traced to the vanishing of the shear component S_{12} in the vicinity of the moving wall, that leads to the degeneracy towards zero of the 3 basis tensors of EB-EASM #1; whereas, in EB-EASM #2, the tensor $\boldsymbol{M}$ is independent on the mean flow.

6 Conclusions

The introduction of the elliptic blending strategy into explicit algebraic stress models was presented. The extended integrity basis due to the introduction of the wall-normal-sensitive tensor in the algebraic relation led to a number of possible approximated formulations. The validation of selected models, for several cases of Poiseuille and Couette-Poiseuille flows, has shown satisfactory behavior, and that the main properties of the underlying Elliptic Blending Reynolds-Stress Model are preserved.

The possibility of building models linear in the mean velocity gradients but resolving the anisotropy is attractive from a numerical robustness standpoint. The 2-term linear model appears as a very acceptable simplified model, with many similarities with the $\overline{v^2}$–f model, but derived from an approach valid in general configurations, and with only 3 differential equations for k, ε and α.

References

1. S. Hoyas and J. Jimenez. Scaling of velocity fluctuations in turbulent channels up to $Re_\tau = 2000$. *Phys. Fluids*, 18(1), 2006.
2. R. Manceau. An improved version of the Elliptic Blending Model. Application to non-rotating and rotating channel flows. In *Proc. 4th Int. Symp. Turb. Shear Flow Phenomena, Williamsburg, VA, USA*, 2005.
3. R. Manceau, J. R. Carlson, and T. B. Gatski. A rescaled elliptic relaxation approach: neutralizing the effect on the log layer. *Phys. Fluids*, 14(11):3868–3879, 2002.
4. R. Manceau and K. Hanjalić. Elliptic blending model: A new near-wall Reynolds-stress turbulence closure. *Phys. Fluids*, 14(2):744–754, 2002.
5. R. D. Moser, J. Kim, and N. N. Mansour. Direct numerical simulation of turbulent channel flow up to $Re_\tau = 590$. *Phys. Fluids*, 11(4):943–945, 1999.
6. P. Orlandi. Database of turbulent channel flow with moving walls. http://dma.ing.uniroma1.it/users/orlandi, 2008.
7. S. B. Pope. A more general effective viscosity hypothesis. *J. Fluid Mech.*, 72:331–340, 1975.
8. C. L. Rumsey, T. B. Gatski, and J. H. Morrison. Turbulence model predictions of strongly curved flow in a U-duct. *AIAA J.*, 38(8):1394–1402, 2000.
9. A. J. M. Spencer. Theory of invariants. In A. C. Eringen, editor, *Continuum Physics*, volume 1. Academic Press, New York, 1971.
10. C. G. Speziale, S. Sarkar, and T. B. Gatski. Modeling the pressure-strain correlation of turbulence: an invariant dynamical system approach. *J. Fluid Mech.*, 227:245–272, 1991.